

## Supporting Information

### High Curie Temperature and Half-metallicity in Atomically Thin Main Group Based Boron Phosphide System: Long Range Ferromagnetism

Gargee Bhattacharyya,<sup>†</sup> Indrani Choudhuri,<sup>#</sup> Biswarup Pathak,<sup>†,#,\*</sup>

<sup>†</sup> Discipline of Metallurgy Engineering and Materials Science, <sup>#</sup>Discipline of Chemistry, School of Basic Sciences and, Indian Institute of Technology (IIT) Indore, Indore, Madhya Pradesh, 453552, India

Email: [biswarup@iiti.ac.in](mailto:biswarup@iiti.ac.in)

#### Contents:

**Text S1.** Computational Details.

**Table S1:** Bader charge analysis of pure BP and Mg<sup>P</sup>@BP.

**Figure S1:** Spin Density Distribution of (a) BP monolayer with single B-vacancy, (b) Be<sup>B</sup>@BP system and (c) Mg<sup>B</sup>@BP.

**Figure S2:** Optimized structure and TDOS of (a) Li<sup>B</sup>@BP with 6.25% doping concentration. The Fermi level is shifted to zero and indicated by a blue dashed line. B, P and Li atoms are indicated by green, gray and pink color respectively. Doped Li atom is indicated by red circle.

**Figure S3:** Optimized structure and TDOS of (a) C<sup>B</sup>@BP (b) C<sup>P</sup>@BP with 6.25% doping concentration. The Fermi level is shifted to zero and indicated by a blue dashed line. B, P and C atoms are indicated by green, gray and brown color respectively. Doped C atom is indicated by red circle.

**Figure S4:** Optimized structure and TDOS of (a) N<sup>B</sup>@BP (b) N<sup>P</sup>@BP with 6.25% doping concentration. The Fermi level is shifted to zero and indicated by a blue dashed line. B, P and N atoms are indicated by green, gray and bluish silver color respectively. Doped N atom is indicated by red circle.

**Figure S5:** Optimized structure and TDOS of (a) Al<sup>B</sup>@BP (b) Al<sup>P</sup>@BP with 6.25% doping concentration. The Fermi level is shifted to zero and indicated by a blue dashed line. B, P and Al atoms are indicated by green, gray and light blue color respectively. Doped Al atom is indicated by red circle.

**Figure S6:** Optimized structure and TDOS of (a)  $\text{Si}^{\text{B}}@\text{BP}$  (b)  $\text{Si}^{\text{P}}@\text{BP}$  with 6.25% doping concentration. The Fermi level is shifted to zero and indicated by a blue dashed line. B, P and Si atoms are indicated by green, gray and dark blue color respectively. Doped Si atom is indicated by red circle.

**Figure S7:** Optimized structure and TDOS of (a)  $\text{S}^{\text{B}}@\text{BP}$  (b)  $\text{S}^{\text{P}}@\text{BP}$  with 6.25% doping concentration. The Fermi level is shifted to zero and indicated by a blue dashed line. B, P and S atoms are indicated by green, gray and yellow color respectively. Doped S atom is indicated by red circle.

**Table S2:** Doping concentration (%), Formation energy/dopant ( $E_F$ ), magnetic moments /dopant ( $\mu\text{B}$ ) and Band gap (eV) for the magnetic systems  $\text{Li}^{\text{P}}@\text{BP}$ ,  $\text{Na}^{\text{B}}@\text{BP}$ ,  $\text{Na}^{\text{P}}@\text{BP}$ ,  $\text{Be}^{\text{P}}@\text{BP}$  and  $\text{Mg}^{\text{P}}@\text{BP}$  systems.

**Figure S8:** TDOS plot of (Mg-B3) unit (Figure 5, manuscript) in  $\text{Mg}^{\text{P}}@\text{BP}$  system. The Fermi level is shifted to zero and indicated by a blue dashed line.

**Figure S9:** (a) Spin density distribution (SDD) (isosurface value:  $0.0005 \text{ e } \text{\AA}^{-3}$ ), (b) TDOS plot, (c)-(e) PDOS plots of Be, B and P atoms of  $\text{Be}^{\text{P}}@\text{BP}$  (6.25%). The Fermi level is shifted to zero and indicated by a blue dashed line.

**Table S3:** Optimized spatial separation between two dopants ( $\text{\AA}$ ), Optimized structure, Exchange energy (meV) and Magnetic ground state of  $\text{Be}^{\text{P}}@\text{BP}$  systems are tabulated.

**Figure S10:** Spin density distribution (SDD) (isosurface value:  $0.0012 \text{ e } \text{\AA}^{-3}$ ) of (a) FM and (b) AFM configuration of  $\text{Mg}^{\text{P}}@\text{BP}$  system in a larger ( $10 \times 5 \times 1$ ) BP supercell.

**Figure S11:** Optimized structures, Spin Density Distribution (SDD) (isosurface value:  $0.0012 \text{ e } \text{\AA}^{-3}$ ), and TDOS of (a) FM, (b) AFM-I and (c) AFM-II configuration of  $\text{Mg}^{\text{P}}@\text{BP}$  (6.25%) in  $8 \times 8 \times 1$  BP supercell. The Fermi level is indicated by the blue dashed line.

**Table S4:** Summary of Magnetic Anisotropy Energies in  $\mu\text{eV}/\text{dopant}$  and the EA for  $\text{Mg}^{\text{P}}@\text{BP}$  (6.25%)

**Text S2:** Mean Field Theory (MFT).

**Text S3:** Monte Carlo (MC) Simulation.

**Table S5:** Formation energy/dopant ( $E_F$ ), binding energy/dopant ( $E_B$ ), magnetic moments /dopant ( $\mu\text{B}$ ), Band gap (eV) for  $\text{Be}^{\text{B}}@\text{BP}$  and  $\text{Mg}^{\text{B}}@\text{BP}$  systems.

**Figure S12:** Electron localization function (ELF; maximum saturation level  $1.0 \text{ e } \text{\AA}^{-3}$ , minimum saturation level  $0.0 \text{ e } \text{\AA}^{-3}$ ) of (a)  $\text{Be}^{\text{P}}@\text{BP}$  (6.25%) and (b)  $\text{Mg}^{\text{P}}@\text{BP}$  (6.25%)

**Figure S13:** Optimized structure and phonon dispersion plot of  $\text{Mg}^{\text{P}}@\text{BP}$  (6.25%).

**Figure S14:** Optimized structure and phonon dispersion plot of  $\text{Mg}^{\text{P}}@\text{BP}$  (6.25%) after soft mode relaxation.

**Text S4:** Calculation of mechanical properties.

---



---

### **Text S1. Computational Details**

Energetic stability of the Be and Mg doped boron monolayer sheet is investigated from the formation energy  $E_{F(P-site/B-site)}$  (eV) and binding energy  $E_B$  (eV). The formation energy calculations are carried out using the following equations<sup>1</sup>

$$E_{F(P-site)} = (E_{Be/Mg@BP} - E_{BP}) - (\mu_{Be/Mg(Bulk)} - \mu_{P(Bulk)}) \quad (1)$$

$$E_{F(B-site)} = (E_{Be/Mg@BP} - E_{BP}) - (\mu_{Be/Mg(Bulk)} - \mu_{B(Bulk)}) \quad (2)$$

Where  $E_{Be/Mg@BP}$  is total energy of the Be / Mg doped BP monolayer system,  $E_{BP}$  is the total energy of undoped BP monolayer,  $\mu_{Be/Mg(Bulk)}$ ,  $\mu_{P(Bulk)}$  and  $\mu_{B(Bulk)}$  are the chemical potential of Be / Mg atom, P atom and B atom from their respective bulk structures.<sup>2-5</sup>

Binding energy refers to the energy required to isolate single Be or Mg atom from Be<sup>P</sup>@BP and Mg<sup>P</sup>@BP systems. Therefore, we have considered the energy of single isolated Be and Mg atom while calculating the binding energy. Binding energy is calculated by the following equation<sup>1</sup>

$$E_B = E_{Be/Mg@BP} - (E_{BP} + E_{Be/Mg(single\ atom)}) \quad (3)$$

Where  $E_{Be/Mg@BP}$  is total energy of the Be / Mg doped BP monolayer system,  $E_{BP}$  is the total energy of undoped BP monolayer,  $E_{Be/Mg(single\ atom)}$  is the total energy of isolated Be / Mg atom.

Cohesive energy of Be and Mg bulk systems are calculated from the following equation

$$E_{Coh} = \frac{E_{Be/Mg(Bulk)} - N \times E_{Be/Mg(single\ atom)}}{N} \quad (4)$$

Furthermore, to predict the magnetic ground state of Be<sup>P</sup>@BP and Mg<sup>P</sup>@BP ML system, we have calculated the exchange energy<sup>1,6-8</sup> ( $E_{ex}$ ) per unit cell and magnetic anisotropic energy<sup>1,6-8</sup> using 8×4×1 supercell of Be and Mg doped BP monolayer. The exchange energy per supercell ( $E_{ex}$ ) is calculated using the following equation where  $E_{FM}$  and  $E_{AFM}$  denotes the energies of ferromagnetic and antiferromagnetic states.

$$E_{ex} = E_{AFM} - E_{FM} \quad (5)$$

Similarly, magnetic anisotropic energy (MAE)<sup>9</sup> per unitcell is calculated incorporating spin-orbit coupling (SOC) effect using the following equation where  $E_{HA}$  is the energy of the system (along hard axis) with application of magnetic field along magnetizing direction (100), (010), (110), (111) and (001).  $E_{EA}$  is the energy of the system in present of a magnetic easy axis, which is an energetically favorable direction for spontaneous magnetization. We have also tried two out of plane direction (001) and (111) magnetizing direction.

$$MAE = E_{HA} - E_{EA} \quad (6)$$

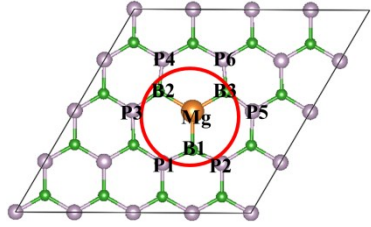
The spin density distribution (SDD)<sup>10</sup> is plotted to understand the nature of electron spin density on the unpaired electron in the Be<sup>P</sup>@BP and Mg<sup>P</sup>@BP ML system. The SDD is calculated using the following equation

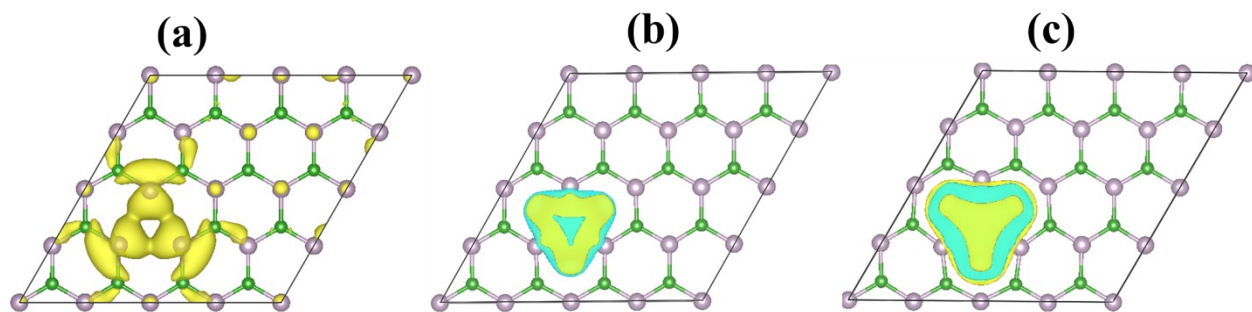
$$\rho_{SD} = \rho_{up} - \rho_{down} \quad (7)$$

Here,  $\rho_{up}$  and  $\rho_{down}$  are the up and down electron spin density, respectively. In the SD, the wave functions for different lobes are indicated by yellow colors. The direct mapping of the electron

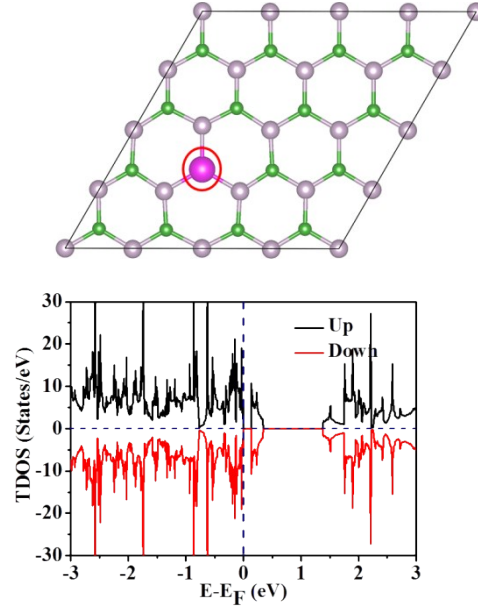
spin density is measured by the neutron diffraction in electron spin resonance (ESR) spectroscopy.<sup>11</sup>

**Table S1: Bader charge analysis of pure BP and Mg<sup>P</sup>@BP.**

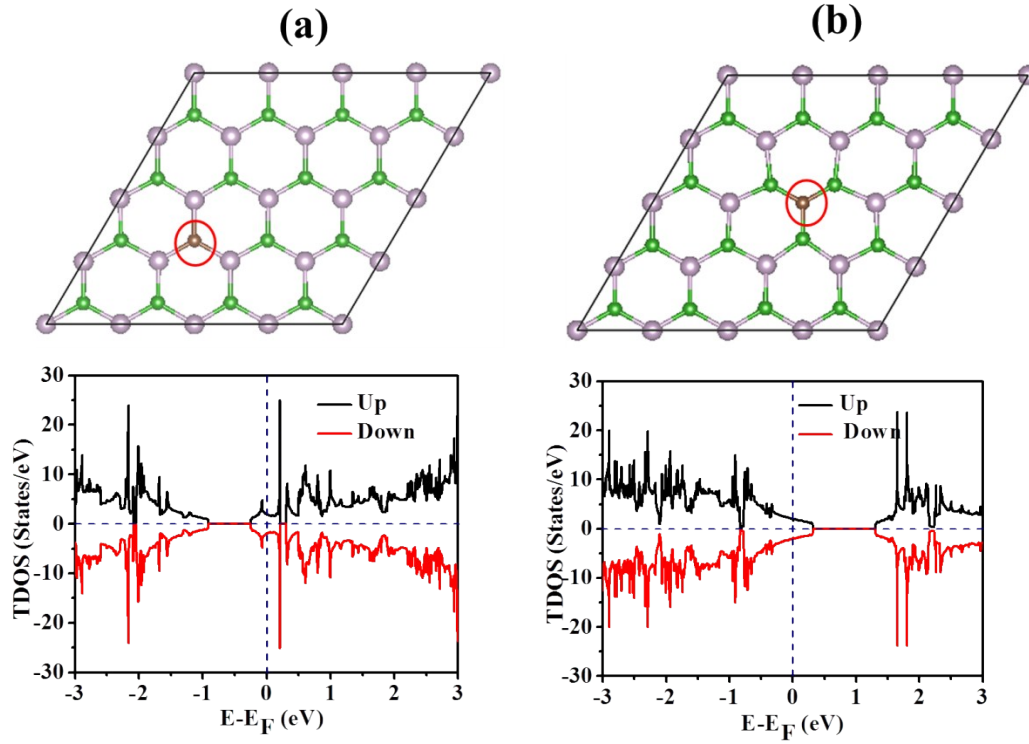
System: Pure BP	Net Effective Charge (Average)		
	<b>B</b>		<b>P</b>
	B = +0.79		P = -0.79
System: Mg <sup>P</sup> @BP			
	Mg	B	P
 5e in Mg-B3 unit	+1.43	B1=+0.38, B2=+0.38 and B3=+0.39	P1=-0.78, P2=-0.81, P3=-0.78, P4=-0.81, P5=-0.79 and P6=- 0.79



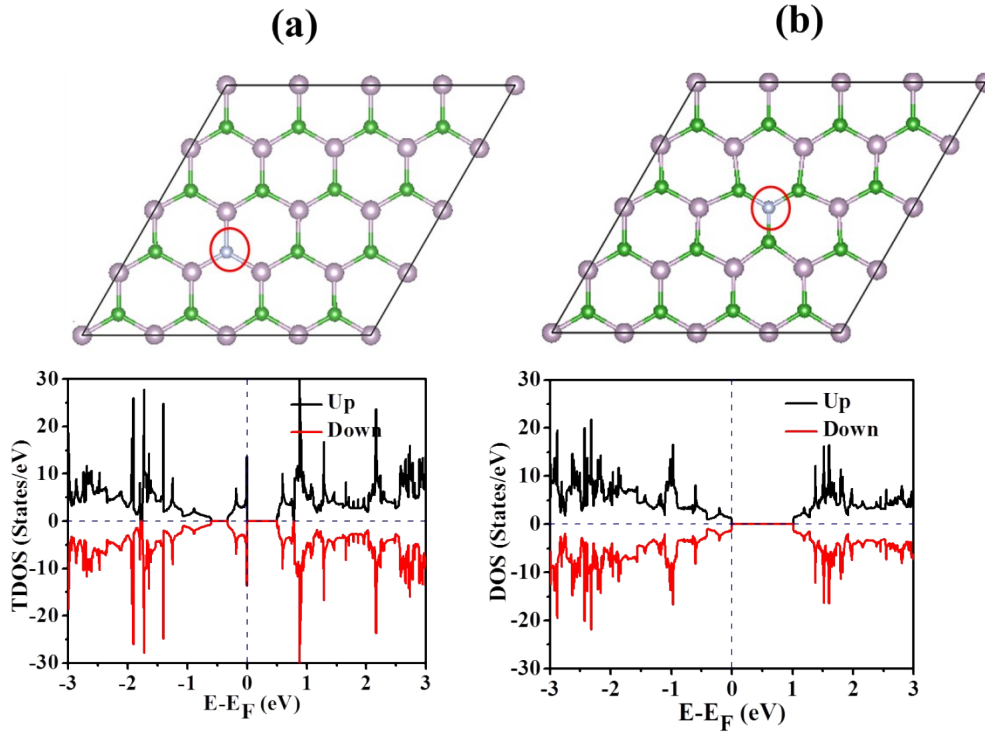
**Figure S1:** Spin Density Distribution of (a) BP monolayer with single B-vacancy, (isosurface value: 0.002337 e Å<sup>-3</sup>) (b) Be<sup>B</sup>@BP system (isosurface value: 5.0 e<sup>-8</sup> Å<sup>-3</sup>) and (c) Mg<sup>B</sup>@BP (isosurface value: 1.0 e<sup>-8</sup> Å<sup>-3</sup>).



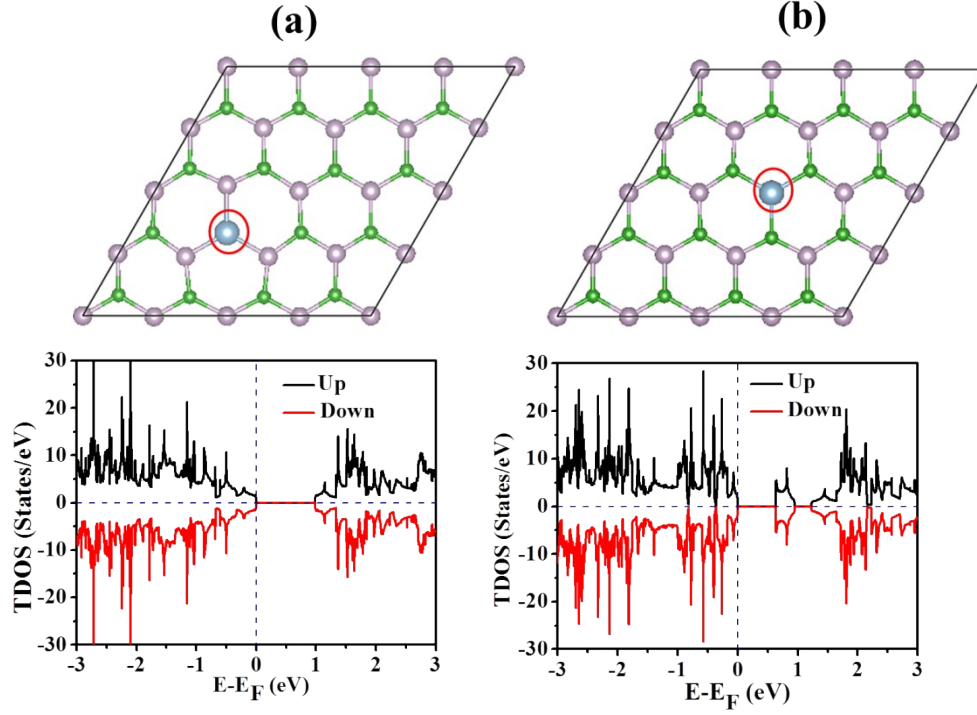
**Figure S2:** Optimized structure and TDOS of (a)  $\text{Li}^{\text{B}}\text{@BP}$  with 6.25% doping concentration. The Fermi level is shifted to zero and indicated by a blue dashed line. B, P and Li atoms are indicated by green, gray and pink color respectively. Doped Li atom is indicated by red circle.



**Figure S3:** Optimized structure and TDOS of (a)  $C^B@BP$  (b)  $C^P@BP$  with 6.25% doping concentration. The Fermi level is shifted to zero and indicated by a blue dashed line. B, P and C atoms are indicated by green, gray and brown color respectively. Doped C atom is indicated by red circle.

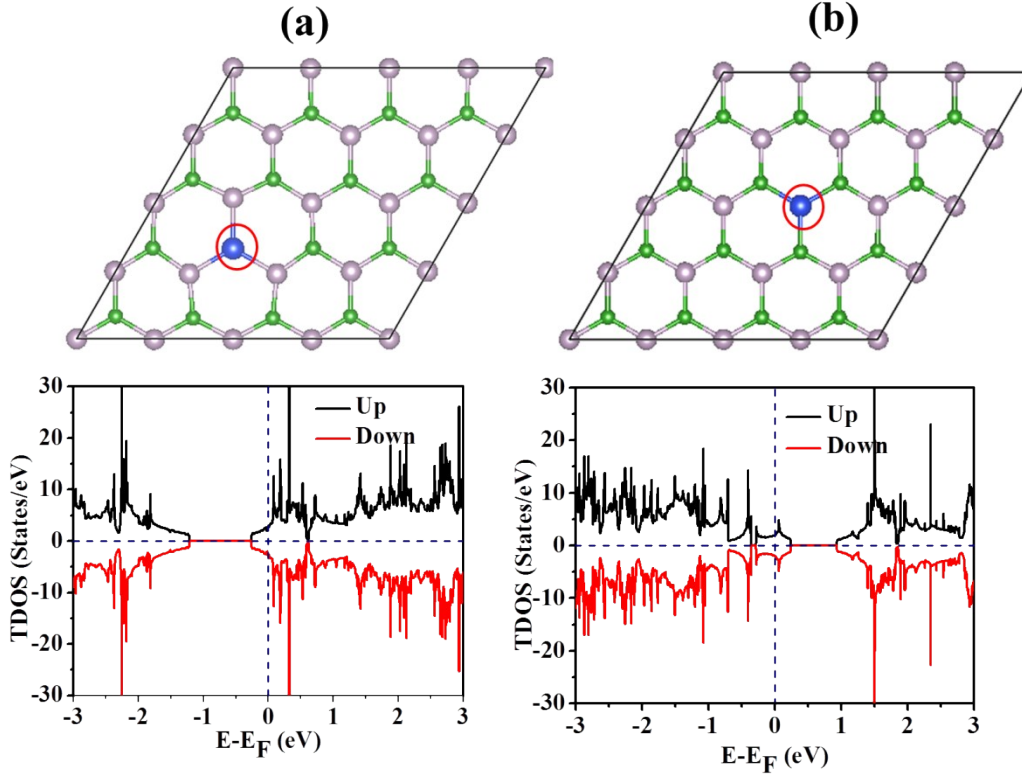


**Figure S4:** Optimized structure and TDOS of (a)  $N^B@BP$  (b)  $N^P@BP$  with 6.25% doping concentration. The Fermi level is shifted to zero and indicated by a blue dashed line. B, P and N atoms are indicated by green, gray and bluish silver color respectively. Doped N atom is indicated by red circle.

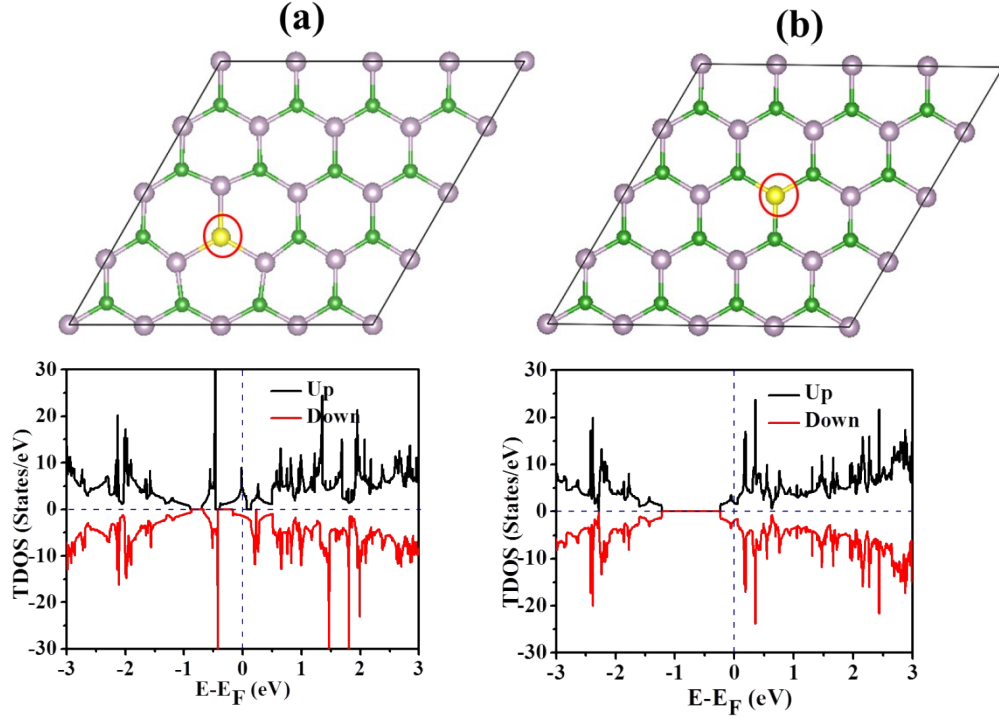


**Figure S5:** Optimized structure and TDOS of (a)  $\text{Al}^{\text{B}}\text{@BP}$  (b)  $\text{Al}^{\text{P}}\text{@BP}$  with 6.25% doping concentration. The Fermi level is shifted to zero and indicated by a blue dashed line. B, P and Al atoms are indicated by green, gray and light blue color respectively. Doped Al atom is indicated by red circle.





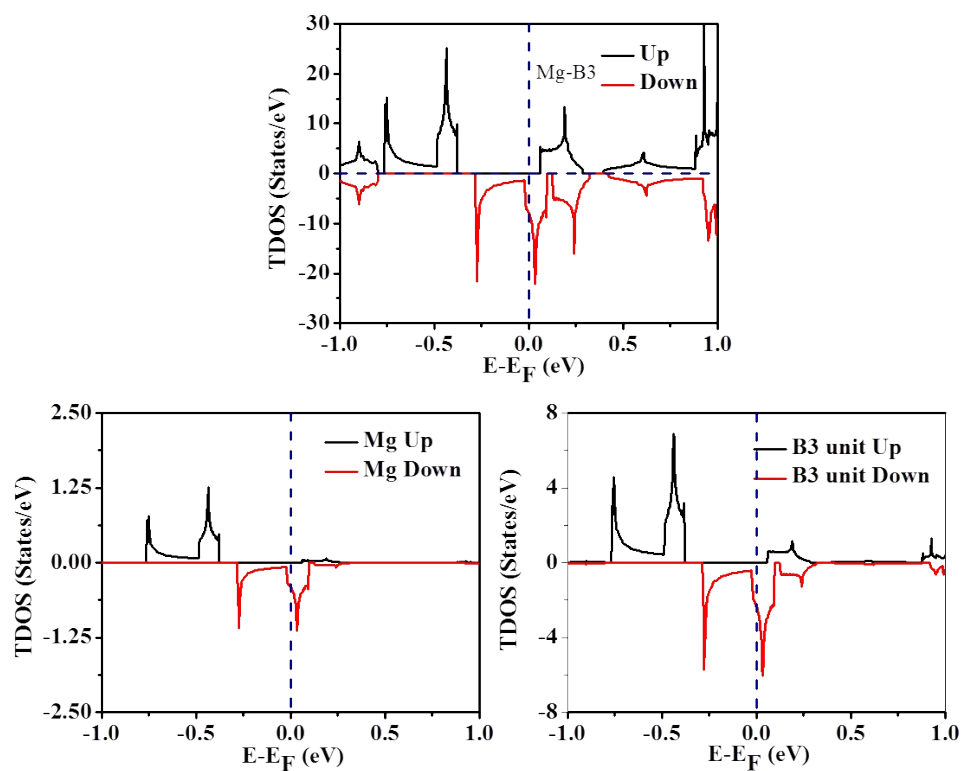
**Figure S6:** Optimized structure and TDOS of (a)  $\text{Si}^{\text{B}}@\text{BP}$  (b)  $\text{Si}^{\text{P}}@\text{BP}$  with 6.25% doping concentration. The Fermi level is shifted to zero and indicated by a blue dashed line. B, P and Si atoms are indicated by green, gray and dark blue color respectively. Doped Si atom is indicated by red circle.



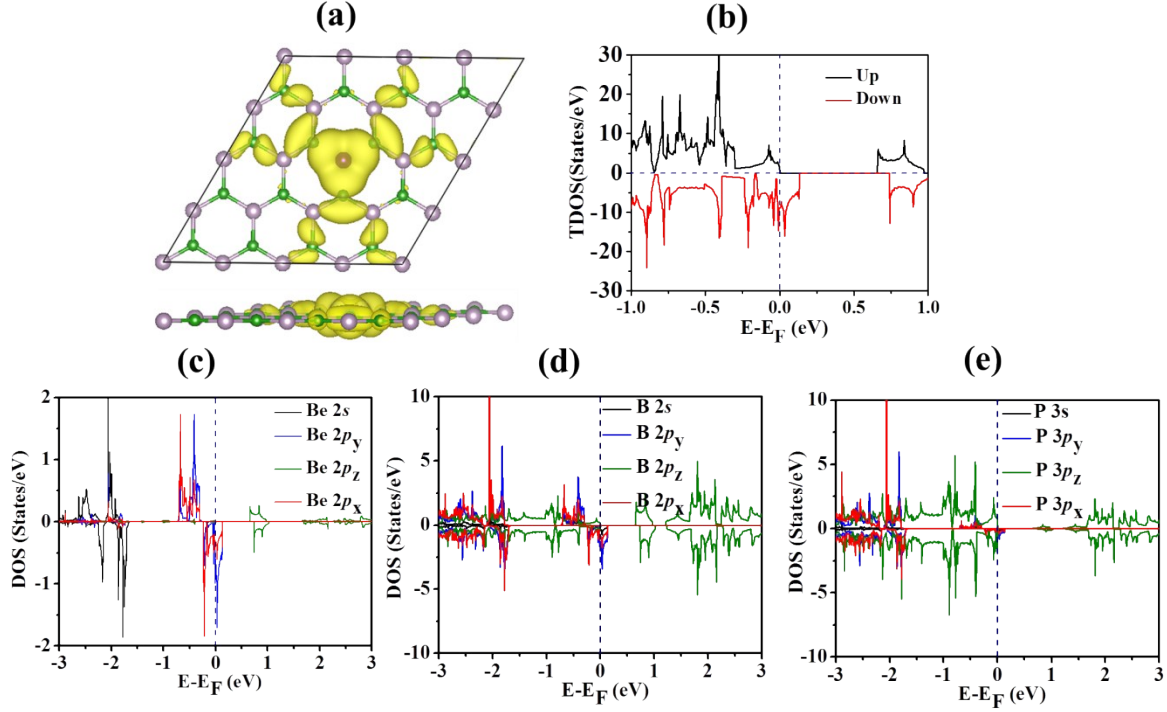
**Figure S7:** Optimized structure and TDOS of (a)  $S^B@BP$  (b)  $S^P@BP$  with 6.25% doping concentration. The Fermi level is shifted to zero and indicated by a blue dashed line. B, P and S atoms are indicated by green, gray and yellow color respectively. Doped S atom is indicated by red circle.

**Table S2:** Doping concentration (%), Formation energy/dopant ( $E_F$ ), magnetic moments /dopant ( $\mu_B$ ) and Band gap (eV) for the magnetic systems  $Li^P@BP$ ,  $Na^B@BP$ ,  $Na^P@BP$ ,  $Be^P@BP$  and  $Mg^P@BP$  systems.

System	Doping concentration (%)	Formation energy (eV/atom)	Magnetic moment/dopant ( $\mu_B$ )	Nature	Spin-Up Gap
$Li^P@BP$	6.25	5.99	2.00	Weak Half-Metallic	0.53
$Na^B@BP$	6.25	6.00	2.00	Half-Metallic	1.02
$Na^P@BP$	6.25	7.21	2.00	Semiconducting	-
$Be^P@BP$	6.25	4.62	0.99	Half-Metallic	0.65
$Mg^P@BP$	6.25	5.46	1.00	Half-Metallic	0.44

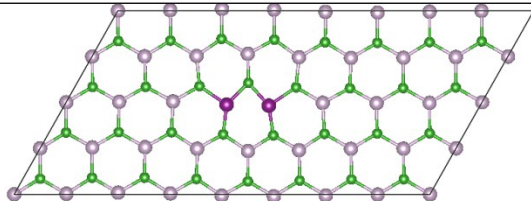
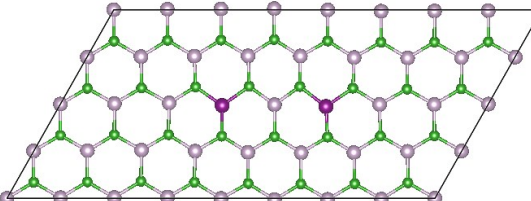


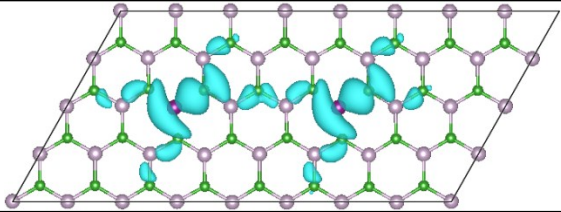
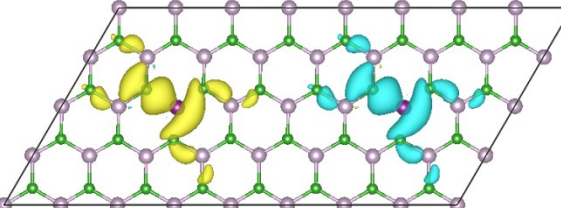
**Figure S8:** TDOS plot of (Mg-B3) unit (Figure 4, manuscript) in  $\text{Mg}^{\text{P}}\text{@BP}$  system. The Fermi level is shifted to zero and indicated by a blue dashed line.



**Figure S9:** (a) Spin density distribution (SDD) (isosurface value:  $0.0005 \text{ e } \text{\AA}^{-3}$ ), (b) TDOS plot, (c)-(e) PDOS plots of Be, B and P atoms of  $\text{Be}^{\text{P}}@\text{BP}$  (6.25%). The Fermi level is shifted to zero and indicated by a blue dashed line.

**Table S3:** Optimized spatial separation between two dopants ( $\text{\AA}$ ), Optimized structure, Exchange energy (meV) and Magnetic ground state of  $\text{Be}^{\text{P}}@\text{BP}$  systems are tabulated.

Spatial Separation between dopants ( $\text{\AA}$ )	Optimized Structure of $\text{Be}^{\text{P}}@\text{BP}$	Magnetic Ground State	
2.59 $\text{\AA}$		Non-magnetic (0.00 $\mu\text{B}$ )	
6.19 $\text{\AA}$		Non-magnetic (0.00 $\mu\text{B}$ )	
		Exchange Energy (meV)	Magnetic Ground State

9.62 Å		3.29	Ferromagnetic
12.84 Å		18.95	Antiferromagnetic

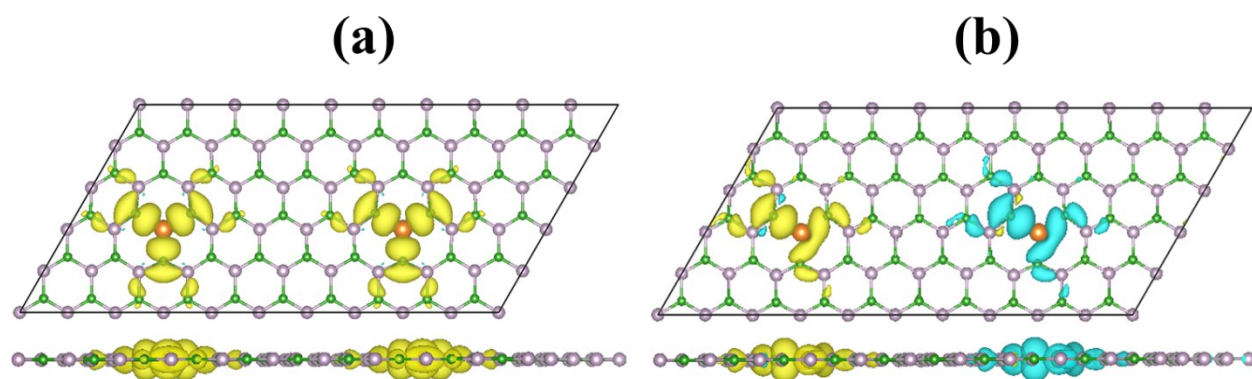


**Figure S10:** Spin density distribution (SDD) (isosurface value:  $0.0012 \text{ e } \text{\AA}^{-3}$ ) of (a) FM and (b) AFM configuration of  $\text{MgP@BP}$  system in a larger ( $10 \times 5 \times 1$ ) BP supercell.

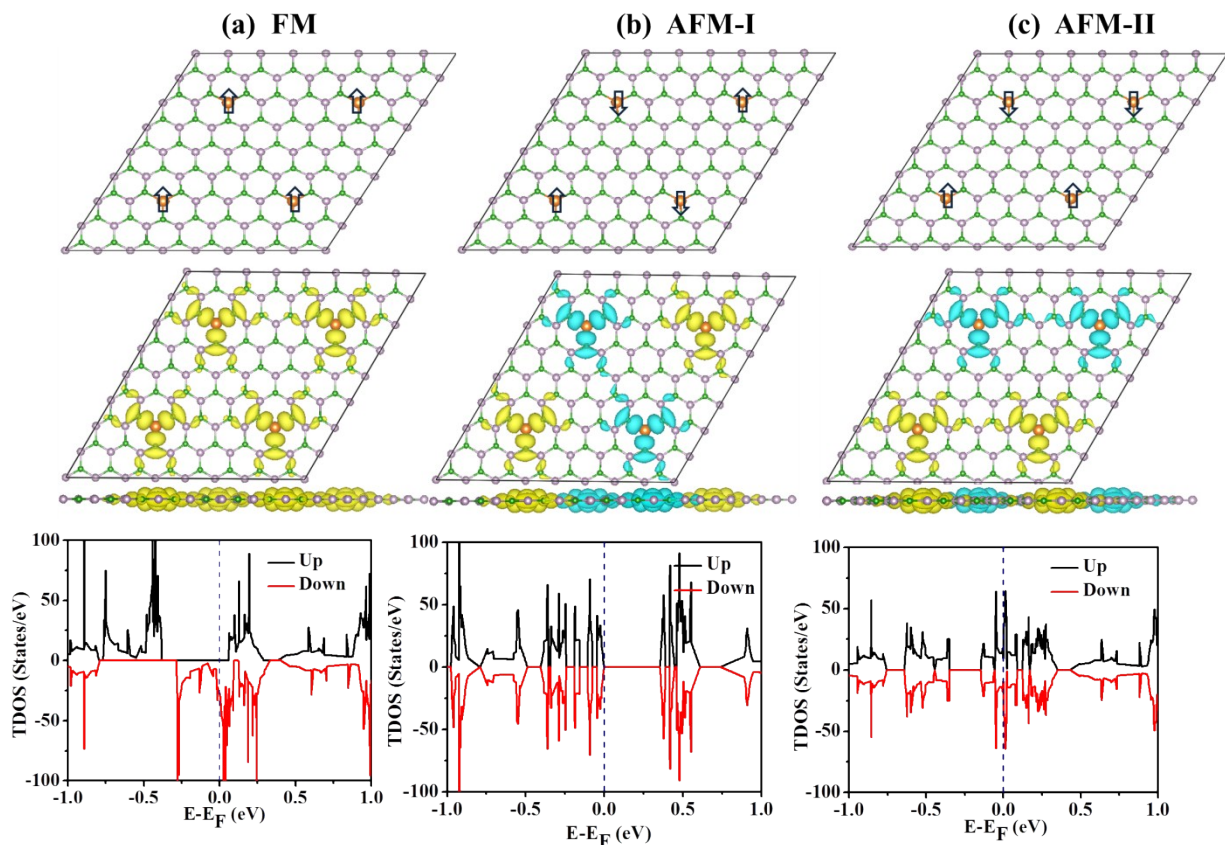


**Figure S11:** Optimized structures, Spin Density Distribution (isosurface value:  $0.0012 \text{ e } \text{\AA}^{-3}$ ), and TDOS of (a) FM, (b) AFM-I and (c) AFM-II configuration of MgP@BP (6.25%) in  $8 \times 8 \times 1$  BP supercell. The Fermi level is indicated by the blue dashed line.

**Table S4:** Summary of Magnetic Anisotropy Energies in  $\mu\text{eV}/\text{dopant}$  and the EA for MgP@BP (6.25%)

MgP@BP (6.25%)	Easy Axis (001)	(100)-(001)	(010)-(001)	(110)-(001)	(111)-(001)
	0	21.6	21.6	21.6	14.2

### Text S2: Mean Field Theory (MFT)

We have taken the MFT approach to calculate the Curie temperature for the two dimensional MgP@BP system. This method has been previously used by Li *et al.*<sup>12</sup> for the Curie temperature calculation for Mn-phthalocyanine (MnPc) system. The main idea behind MFT method is to replace all interactions to any one body with an average or effective interaction.<sup>13</sup> It reduces any

multi-body problem into an effective one-body problem. The detailed partition function can be written as follows,

$$Z = \sum_{m=-M, -M+2, \dots, M-2, M} e^{\gamma J m \langle M \rangle / K_B T} \quad (8)$$

Here, the “J” is the exchange parameter, “ $\gamma$ ” is the coordination number, “m” is the ensemble average magnetic moment, and “M” is the calculated magnetic moment of Mg-B3 unit.

Thus the average spin of each magnet becomes,

$$Z = \frac{1}{Z} \sum_{m=-M, -M+2, \dots, M-2, M} m \times e^{\gamma J m \langle M \rangle / K_B T} \quad (9)$$

$$P = \frac{\gamma J}{K_B T}$$

Now, we assume that

The above equation can be easily deducible when the parameter ‘P’ varies along with the static solution  $\langle m \rangle$ . At the critical point,

$$P_c = P = \frac{\gamma J}{K_B T} \quad (10)$$

At this critical point, the phase transition of the system between ferromagnetic to paramagnetic occurs. This critical point is known as Curie temperature.

### Text S3: Monte Carlo (MC) Simulation

Monte Carlo simulations involve generating a subset of configurations or samples, chosen using a random algorithm from a configuration space, according to a probability distribution or weight function. Observables are then computed as averages over the samples.<sup>14</sup> One sample or configuration of the magnet is a particular assignment of spin values, say

$$S_1 = +1; S_2 = -1; S_3 = +1; \dots S_{N_s} = +1 \quad (11)$$



in which each spin is set “up” or “down”. According to statistical mechanics, the average value of an observable is got by weighting each configuration with the Boltzmann factor. For example, the average magnetization at some fixed temperature  $T$  is given by,

$$\langle M \rangle = \frac{\sum_{config} M e^{-E/K_B T}}{\sum_{config} e^{-E/K_B T}} \quad (12)$$

**Table S5:** Formation energy/dopant ( $E_F$ ), binding energy/dopant ( $E_B$ ), magnetic moments /dopant ( $\mu_B$ ), Band gap (eV) for  $\text{Be}^B@BP$  and  $\text{Mg}^B@BP$  systems.

<b><math>\text{Be}^B@BP</math> (%)</b>	<b>Formation energy (eV/atom)</b>	<b>Binding Energy (eV/atom)</b>	<b>Magnetic moment /dopant(<math>\mu_B</math>)</b>	<b>Nature</b>	<b>Band Gap (eV)</b>
6.25	1.06	4.03	0.00	Metallic	0
<b><math>\text{Mg}^B@BP</math> (%)</b>					
6.25	3.26	7.99	0.00	Metallic	0

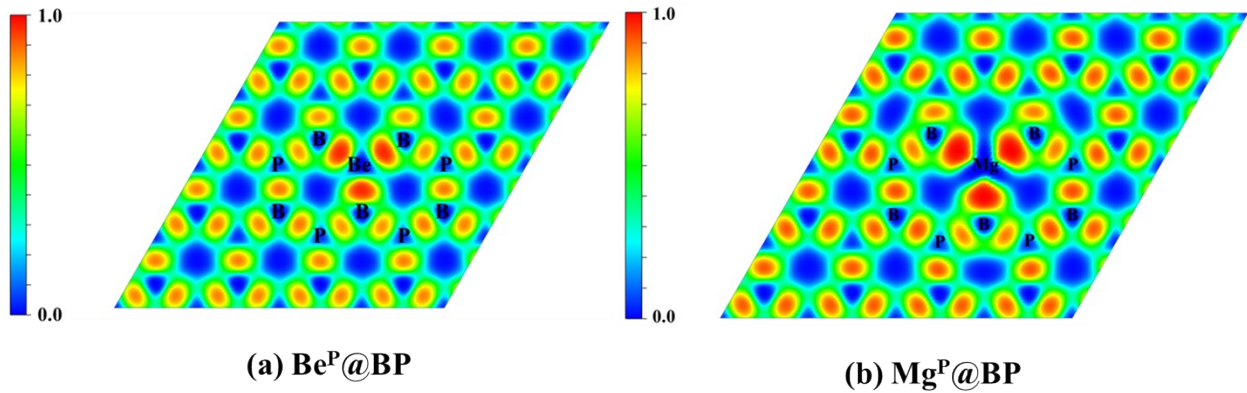


**Figure S12:** Electron localization function (ELF; maximum saturation level  $1.0 \text{ e } \text{\AA}^{-3}$ , minimum saturation level  $0.0 \text{ e } \text{\AA}^{-3}$ ) of (a)  $\text{Be}^P@BP$  (6.25%) and (b)  $\text{Mg}^P@BP$  (6.25%)



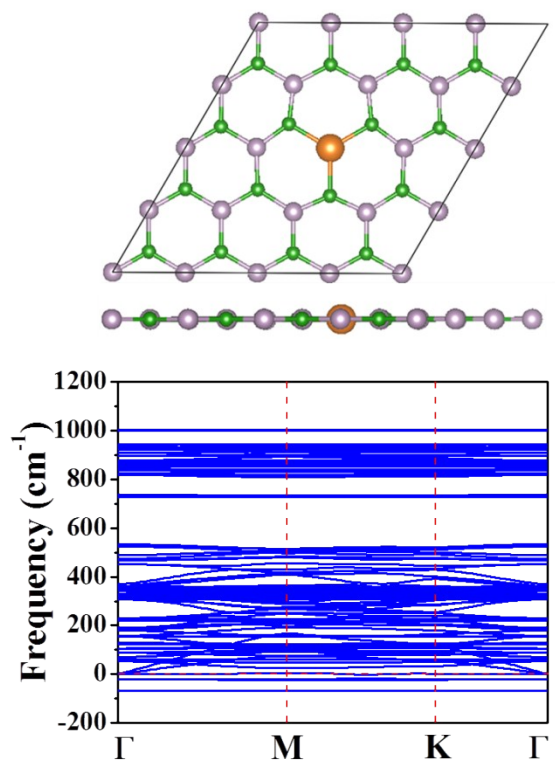


**Figure S13:** Optimized structure and phonon dispersion plot of MgP@BP (6.25%)

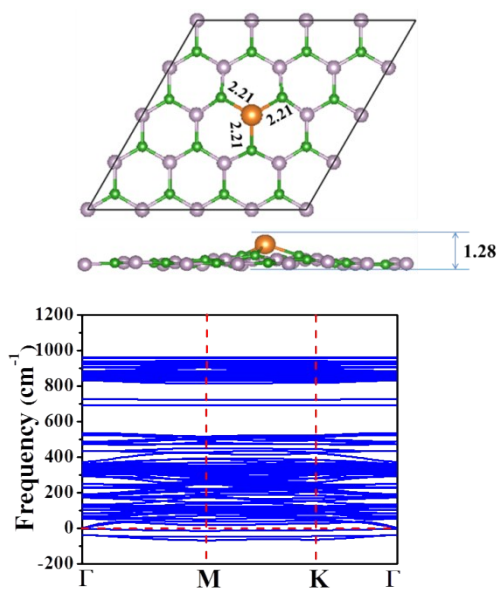


**Figure S14:** Optimized structure and phonon dispersion plot of MgP@BP (6.25%) after soft mode relaxation.

**Text S4:** Calculation of mechanical properties

The Mg<sup>P</sup>@BP (6.25%) sheets can be distorted either by tensile strain (by gradually increasing the lattice parameters) or compressive strain (by gradually reducing the lattice parameters). The percentage (%) of applied strain can be calculated as follows<sup>15</sup>

$$\% \text{ of strain} = \frac{a - a_1}{a} \times 100 \quad (13)$$

Where ‘ $a$ ’ and ‘ $a_1$ ’ are the lattice constants of the Mg<sup>P</sup>@BP (6.25%) sheet before and after the strain.

Tensile stress is applied along the in-plane uniaxial and biaxial directions to evaluate the mechanical stability of Mg<sup>P</sup>@BP (6.25%) sheet. Atomic positions are relaxed at each strain until the forces on each atom are less than  $10^{-2}$  eV Å<sup>-1</sup>. The effects of uniaxial and biaxial strains are examined on a supercell (4×4×1) of 32 atoms. Elastic limit is calculated from the stress-strain curve under the tensile stretch [Figure 8c, Manuscript].<sup>16</sup>

Further, the mechanical properties of the Mg<sup>P</sup>@BP (6.25%) sheet can be calculated from the strain vs. strain energy plot [Figure 8d, Manuscript]. The elastic energy (U/per unit cell) near the equilibrium position can be calculated using the following formula:

$$U = \frac{1}{2}C_{11}\varepsilon_{xx}^2 + \frac{1}{2}C_{22}\varepsilon_{yy}^2 + C_{12}\varepsilon_{xx}\varepsilon_{yy} + 2C_{44}\varepsilon_{xy}^2 \quad (14)$$

Where  $C_{11}$ ,  $C_{22}$ ,  $C_{22}$  and  $C_{22}$  are the linear elastic constants, whereas the  $\varepsilon_{xx}$ ,  $\varepsilon_{yy}$  and  $\varepsilon_{xy}$  are the in plane stress along x, y and xy directions (according to vigot notation)<sup>17</sup> respectively. The value of elastic constants can be calculated from the polynomial fitting of strain vs energy plot.<sup>17-</sup>

<sup>19</sup> The main criteria for mechanical stability are  $C_{11} > C_{12}$  and  $C_{44} > 0$ . Young’s modulus (Y) is calculated using the following formulas.<sup>20</sup>

$$Y = \frac{(C_{11}^2 - C_{22}^2)}{C_{11}} \quad (15)$$

## Reference:

- [1] I. Choudhuri, G. Bhattacharyya, S. Kumar and B. Pathak, *J. Mater. Chem. C*, 2016, **4**, 11530.
- [2] Y.W. Yang and P. Coppens, *Acta Crystallogr.*, 1978, **34A**, 61.
- [3] C. B. Walker and M. Marezio, *Acta Met.*, 1959, **7**, 769.
- [4] L. McCarty, *J. Am. Chem. Soc.*, 1958, **80**, 2592.
- [5] A. Simon, H. Borrmann and H. Craubner, *Phosphorus and Sulfur and the Related Elements*, 1987, **30**, 507.
- [6] I. Choudhuri, S. Kumar, A. Mahata, K. S. Rawat and B. Pathak, *Nanoscale*, 2016, **8**, 14117.
- [7] I. Choudhuri, P. Garg and B. Pathak, *J. Mater. Chem. C*, 2016, **4**, 825
- [8] S. Kumar, I. Choudhuri and B. Pathak, *J. Mater. Chem. C*, 2016, **4**, 9069.
- [9] Y. Sun, Z. Zhuo, X. Wu and J. Yang, *Nano Lett.*, 2017, **17**, 2771–2777.
- [10] A. Schweiger and G. Jeschke, *Principles of Pulse Electron Paramagnetic Resonance*, Oxford University Press, Oxford, England, 2001.
- [11] IUPAC Gold Book.
- [12] X. Li, X. Wu, J. Yang, *J. Am. Chem. Soc.*, 2014, **136**, 5664.
- [13] X. Wang, R. Wu, D. S. Wang, A. J. Freeman, *Phys. Rev. B: Condens. Matter Mater. Phys.*, 1996, **54**, 61.
- [14] D. P. Kroese, T. Brereton, T. Taimre, Z. I. Botev, *Comput. Stat.* 2014, **6**, 386.
- [15] M. Topsakal, S. Ciraci, *Phys. Rev. B: Condens. Matter Mater. Phys.* 2010, **81**, 024107.
- [16] S. Zhang, J. Zhou, Q. Wang, C. Xiaoshuang, K. Yoshiyuki, P. Jena. *Proc. Natl. Acad. Sci. U.S.A.* 2015, **112**, 2372
- [17] R. C. Andrew, R. E. Mapasha, A. M. Ukpong, and N. Chetty. *Phys. Rev. B* 2012, **85**, 125428.
- [18] K. Wright, J. D. Gale. *Phys. Rev B* 2004, **70**, 035211.

[19] Y. Ding, Y. J. Phys. Chem. C 2013, 117, 18266–18278.

[20] J. M. de Sousa, T. Botari, E. Perim, R. A. Bizao, D. S. Galvao, arXiv:1606.01055v1